



# Cavity ring-down spectroscopy sensor development for high-time-resolution measurements of gaseous elemental mercury in ambient air

A. Pierce<sup>1</sup>, D. Obrist<sup>1</sup>, H. Moosmüller<sup>1</sup>, X. Fain<sup>1,2</sup>, and C. Moore<sup>1</sup>

<sup>1</sup>Desert Research Institute, Division of Atmospheric Sciences, Reno, NV, USA

<sup>2</sup>UJF – Grenoble 1/CNRS, Laboratoire de Glaciologie et Géophysique de l'Environnement (LGGE), UMR5183, Grenoble, 38041, France

Correspondence to: A. Pierce (ashley.pierce@dri.edu)

Received: 6 November 2012 – Published in Atmos. Meas. Tech. Discuss.: 21 December 2012

Revised: 20 April 2013 – Accepted: 4 May 2013 – Published: 5 June 2013

**Abstract.** We describe further development of a previous laboratory prototype pulsed cavity ring-down spectroscopy (CRDS) sensor into a field-deployable system for high-time-resolution, continuous, and automated measurement of gaseous elemental mercury (GEM) concentrations in ambient air. We employed an external, isotopically enriched Hg cell for automated locking and stabilization of the laser wavelength on the GEM peak absorption during measurements. Further, we describe implementation of differential absorption measurements via a piezoelectric tuning element for pulse-by-pulse tuning of the laser wavelength onto and off of the GEM absorption line. This allowed us to continuously correct (at 25 Hz) for system baseline extinction losses unrelated to GEM absorption.

Extensive measurement and calibration data obtained with the system were based on spike addition in both GEM-free air and ambient air. Challenges and interferences that occurred during measurements (particularly in ambient air) are discussed including temperature and ozone (O<sub>3</sub>) concentration fluctuations, and steps taken to reduce these. CRDS data were highly linear ( $r^2 \geq 0.98$ ) with data from a commercial Tekran 2537 Hg analyzer across a wide range of GEM concentrations (0 to 127 ng m<sup>-3</sup>) in Hg-free and ambient air. Measurements during periods of stable background GEM concentrations provided a conservative instrument sensitivity estimate of 0.35 ng m<sup>-3</sup> for the CRDS system when time averaged for 5 min. This sensitivity, along with concentration patterns observed in ambient air (with the CRDS system and verified with the Tekran analyzer), showed that the

sensor was capable of characterizing GEM fluctuations in ambient air. The value of fast-response GEM measurements was shown by a series of GEM spike additions – highlighting that high-temporal-resolution measurement allowed for detailed characterization of fast concentration fluctuations not possible with traditional analyzers.

## 1 Introduction

Mercury (Hg) is a highly toxic pollutant with an important presence in the atmosphere due to emissions from natural and anthropogenic sources (Schroeder and Munthe, 1998). Atmospheric Hg cycling is particularly important because deposition is the primary source of Hg to many remote ecosystems (Fitzgerald et al., 1998; Lindberg et al., 2007; Rothenberg et al., 2010). Three major forms of atmospheric Hg are currently measured with available analytical techniques: gaseous elemental mercury (GEM), gaseous oxidized mercury (GOM), and particulate-bound mercury (PHg). GEM generally represents more than 90 % of the atmospheric Hg mass, is semi-volatile, and has low solubility in water. As a result, GEM has a long atmospheric residence time (5 to 24 months), can be transported 1000s of km, and is the species predominantly responsible for the global dispersion of Hg (Schroeder and Munthe, 1998; Lamborg et al., 2002; Slemr et al., 1985; Swartzendruber et al., 2006). GOM and PHg, on the other hand, have much shorter atmospheric residence times and are considered to be local or regional pollutants

(Swartzendruber et al., 2006; Schroeder and Munthe, 1998; Shia et al., 1999).

Existing GEM measurement technologies require 2.5 to 5 min of sampling and multiple liters of air to accurately determine ambient air GEM concentrations (Landis et al., 2002; Lyman et al., 2010). The most common GEM measurement technology is cold vapor atomic fluorescence spectroscopy (CVAFS; Clevenger et al., 1997), implemented in commercially available sensors – e.g., the Tekran Model 2537 Mercury Vapor analyzer (Tekran Inc., Toronto, Canada). The technique involves pre-concentration of GEM from several liters of air onto a gold trap. The GEM is thermally desorbed into an inert argon stream and subsequently analyzed free from interferences (e.g., O<sub>3</sub>). Other methods also have been used for measurement of GEM concentrations, including atomic absorption spectrometry (the commercially available OhioLumex system) and laser-induced fluorescence (LIF) spectrometry sensors (Table 1).

The development and availability of fast-response GEM sensors would allow for enhanced characterization of atmospheric Hg dynamics and high-frequency fluctuations that may correspond to sources, sinks, and chemical transformation (e.g., atmospheric mercury depletion events). For example, Bauer et al. (2003) used fast-response (10 Hz, with a 10 s integration time for measurements) pulsed laser photolysis-pulsed laser-induced fluorescence (PLP-PLIF) to estimate kinetics of the reaction between GEM and the hydroxyl radical in the laboratory (a proposed route of GOM formation). A further use of high-frequency GEM measurements is in surface-atmosphere flux measurement techniques such as eddy covariance, a method that requires sensor time resolution of 10 Hz or faster to resolve high-frequency concentration deviations induced by turbulent eddies that occur across time scales ranging from 10<sup>-3</sup> to 10<sup>4</sup> s (Arya, 2001).

Faïn et al. (2010) describe a prototype strictly designed for laboratory use, based on cavity ring-down spectroscopy (CRDS) with high-reflectivity mirrors to create long absorption path lengths in a compact cell (1 m length). The authors present manual wavelength scans including the GEM absorption wavelength of 253.65 nm to characterize GEM concentrations in the laboratory using Hg-free air (i.e., charcoal-filtered air) spiked with GEM to reach concentrations between 0.2 and 573 ng m<sup>-3</sup> (Faïn et al., 2010). In addition, they present preliminary measurements of GEM in ambient air and identify potential interferences by ambient air constituents such as O<sub>3</sub> and particulate matter that absorb in the same wavelength region as GEM.

Several steps were needed to convert the laboratory-based prototype system documented by Faïn et al. (2010) into a field-deployable sensor for high-time-resolution measurement of ambient air GEM. Here, we detail developments of the system such as automatic and reliable laser wavelength positioning (“locking”) onto the peak GEM absorption line with an external, Hg-filled cell (Sect. 3.1); implementation of differential absorption measurements to continuously correct

for baseline system extinction by pulse-to-pulse (i.e., 50 Hz) wavelength detuning (Sect. 3.2); automation of data acquisition and real-time signal processing at 50 Hz (Sect. 3.3); and configuration of the system for field deployment (Sect. 3.4). We then show extensive measurements and GEM spike additions in both Hg-free and ambient air in the urban airshed of Reno, Nevada, compare results to data obtained with a Tekran 2537 sensor, and discuss interferences for CRDS measurements in ambient air (Sect. 4).

## 2 Pulsed cavity ring-down spectroscopy and other methods to measure GEM

### 2.1 Cavity ring-down spectroscopy – overview of theory

Pulsed cavity ring-down spectroscopy is an absorption technique that uses high-reflectivity mirrors positioned at both ends of a high-finesse measurement cavity. A small fraction of the power of each laser pulse is coupled into the cavity through one mirror where it bounces between the two mirrors; multiple reflections of the laser pulse produce long path lengths for absorption measurements leading to greater sensitivity compared to standard absorption measurements (Jongma et al., 1995; Spuler et al., 2000; Atkinson, 2003). In addition, the use of a short cavity allows for small sample volumes (Moosmüller et al., 2005). The laser pulse energy introduced into the cavity decays exponentially with time due to extinction and reflection losses within the cavity. CRDS is used to measure total extinction in the cavity, which is the sum of mirror losses as well as scattering and absorption losses due to particles and gases (Tao et al., 2000; Moosmüller et al., 2005; Atkinson, 2003). The power in the cavity can be quantified by the current signal  $S_t$  of a photomultiplier tube exposed to the light leaking out of the cavity through the second mirror. Equation (1) shows how the signal  $S_t$  decays with time due to various system components:

$$S_t = S_o e^{-\alpha c t} = S_o e^{-[(\alpha_{\text{Hg}} + \alpha_{\text{BG}} + \alpha_{\text{M}}) * c t]}, \quad (1)$$

where  $S_o$  is the signal at  $t = 0$ ;  $\alpha$  is the sum of the wavelength-dependent GEM absorption coefficient including  $\alpha_{\text{Hg}}$  (a wavelength-dependent GEM absorption coefficient),  $\alpha_{\text{BG}}$  (a background extinction coefficient comprised of gaseous and particulate absorption and scattering), and  $\alpha_{\text{M}}$  (a mirror extinction term);  $c$  is the speed of light; and  $t$  is time. If all losses other than those due to GEM ( $\alpha_{\text{BG}}$  and  $\alpha_{\text{M}}$ , termed baseline losses) can be reliably quantified, absorption losses by GEM ( $\alpha_{\text{Hg}}$ ) can be calculated by measuring total extinction losses and subtracting baseline losses. In our system, the extinction loss for each laser pulse ( $\sim 3 \mu\text{s}$  signal decay time) is quantified using real-time exponential fits of the signal (Wheeler et al., 1998).

**Table 1.** Sensors used for detection of GEM.

Product/type	Detection limit ( $3\sigma$ in $\text{ng m}^{-3}$ )	Response time	Made in?	Measurement method	Source
Zeeman mercury analyzer RA-915+ Tekran 2537B	2*	1 s	Ambient air	Atomic absorption spectrometer with Zeeman background correction	OhioLumex (2012)
Lidar	0.5–2*	5–10 s	Lab air, Factory plume	Cold vapor atomic fluorescence spectrometry Differential absorption lidar (DIAL)	Tekran (2009) Edner et al. (1989)
LIF	0.15	10 s	$\text{N}_2$ buffer gas	Sequential two-photon laser-induced fluorescence spectrometry	Bauer et al. (2002, 2003)
CRDS	27	3 s	Lab air	BBO crystal frequency-doubled, pulsed dye laser (line width of $0.1 \text{ cm}^{-1}$ ) pumped (10 Hz) by a frequency-tripled Nd:YAG laser at 355 nm	Jongma et al. (1995)
CRDS	4.5	75 s	Lab air, Perm source and $\text{N}_2$	Quanta-Ray GCR-16 Nd:YAG laser pumping a PDL-3 dye laser with 10 Hz repetition rate, BBO frequency doubled ( $0.11 \text{ cm}^{-1}$ line width)	Spuler et al. (2000)
CRDS	24	unspecified	Argon	Nd:YAG laser pumping a tunable dye laser frequency doubled ( $0.1 \text{ cm}^{-1}$ line width)	Tao et al. (2000)
CRDS	90*	10 s	Flue gas	Frequency-tripled Alexandrite laser, seeded with a single mode, external-cavity diode laser, UV output line width $0.006 \text{ cm}^{-1}$	Carter (2004)
(Microwave-induced plasmas) MIP-CRDS	400*	5 s	Argon	Alternative plasma sources for CRDS measurement of GEM (tube-shaped MIP source) using Nd:YAG laser with 20 Hz repetition rate pumping a dye laser (line width $0.08 \text{ cm}^{-1}$ )	Duan et al. (2005)
(Microwave-induced plasmas) MIP-CRDS	$\sim 1841$	2–5 s	Argon	Alternative plasma sources for CRDS measurements, Nd:YAG laser with 20 Hz repetition rate pumping a dye laser frequency doubled (line width $0.08 \text{ cm}^{-1}$ )	Wang et al. (2005)
CRDS	2.19	0.02 s	Ambient Air	Nd:YAG laser pumping a tunable dye laser ( $0.00019 \text{ nm}$ line width)	Faïn et al. (2010)
CEAS	66	10 s	Injections into static cell	Cavity-enhanced absorption spectroscopy, Hg-Ne pencil lamp	Darby et al. (2012)

\* Definition of detection limit not specified (i.e., not necessarily  $3\sigma$ ).

## 2.2 Previous CRDS laboratory prototype

The laboratory prototype that we have further refined is described in detail in Faïn et al. (2010). It operates at UV laser wavelengths at and near peak absorption for GEM (253.65 nm; Spuler et al., 2000). These laser pulses are created by a Quanta Ray, Q-switched Nd:YAG pump laser (Newport-Spectra-Physics, Mountain View, CA, USA) operating at a fundamental wavelength of 1064 nm with a frequency-tripled output of 355 nm. This laser pumps a dye laser (Model Sirah Cobra, Sirah Laser- und Plasmatechnik GmbH, Kaarst, Germany) to generate a frequency-doubled output tunable between 215 and 280 nm. Short (5 ns) laser pulses are directed into a 1 m long closed-path cavity built with two 99.895 % reflectivity mirrors (MLD Technologies, Mountain View, CA, USA). Using an external, low-pressure

Hg cell system and two photodiodes (PDs; DET10M, Thorlabs, Newton, NJ, USA), the laser wavelength is determined relative to the GEM absorption line. In Faïn et al. (2010), manual scans by the laser operator were performed to characterize the GEM absorption spectra, and measurements of GEM concentrations were performed by scanning the laser wavelength to the peak absorption of one of five resolvable isotopes of Hg (Fig. 1a, blue line) for 10 s and then scanning of the absorption line for another 10 s to quantify system baseline extinction. This scanning procedure took 5–10 min (depending on scan step sizes) and therefore, despite using a fast-pulsed laser, did not allow for high-time-resolution measurements. Below, we describe the development steps performed for automated operation of the system at high temporal resolution and system deployment in the field.

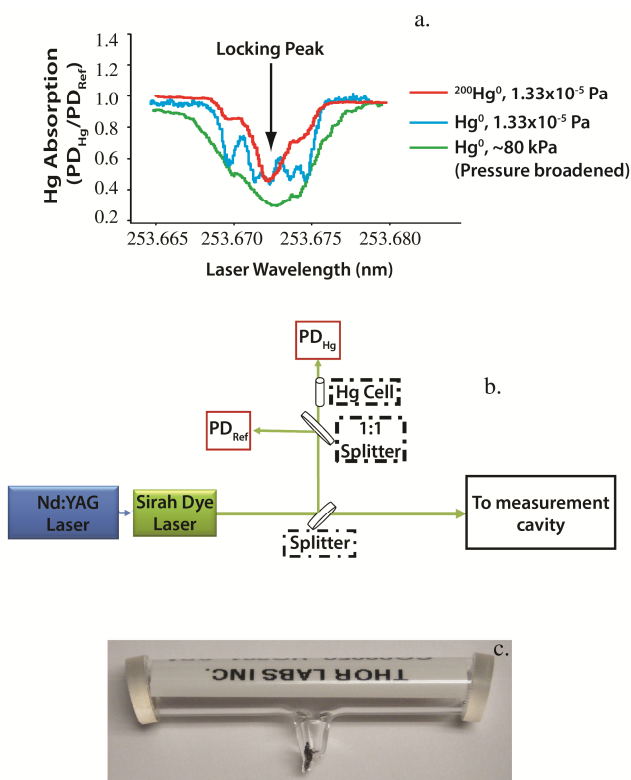


**Fig. 1.** (a) Absorption spectra of external Hg cells filled with metallic Hg ( $\sim 80$  kPa air and  $1.33 \times 10^{-5}$  Pa Hg pressure) and filled with isotopically enriched  $^{200}\text{Hg}$  at  $1.33 \times 10^{-5}$  Pa pressure, plotted on a normalized y scale to compare different scans. Note that absolute wavelength numbers in figure are only approximations based on laser tuning grating position. (b) Schematic diagram of the experimental setup including the Hg cell and position of two photodiodes (PD) for control and locking of laser wavelength. (c) External quartz Hg cell filled with  $^{200}\text{Hg}$  for wavelength locking of the laser system.

### 2.3 Other GEM measurement techniques

A series of GEM measurement techniques have been developed and discussed in the literature (Table 1). The technique most used in research and ambient air monitoring is the Tekran 2537 analyzer, which has been tested in various inter-comparison studies (Ebinghaus et al., 1999; Munthe et al., 2001; Pandey et al., 2011; Schroeder et al., 1995). The system has excellent sensitivity ( $0.1 \text{ ng m}^{-3}$  ( $3\sigma$ ) over 5 min) and stability in laboratory and ambient air measurements (Tekran, 2009). Other techniques include a portable atomic absorption spectroscopy system using Zeeman background correction with a sensitivity of  $2 \text{ ng m}^{-3}$  for 1 s; measurements by this system have been made in laboratory and ambient air (OhioLumex, 2012). Another system is based on differential absorption lidar (DIAL) with a sensitivity of  $0.5\text{--}2 \text{ ng m}^{-3}$  for 5 to 10 s in laboratory air and factory plume measurements (Edner et al., 1989). A sequential two-photon

laser-induced fluorescence (LIF) spectrometer with a 10 Hz laser system and sensitivity of  $0.15 \text{ ng m}^{-3}$  ( $3\sigma$ ) for 10 s also has been employed for laboratory air and ambient air measurements (Bauer et al., 2002, 2003). Other CRDS systems, with sensitivities ranging from  $2.19$  to  $27 \text{ ng m}^{-3}$ , operating at  $10\text{--}50$  Hz have been used to measure GEM in the laboratory, inert gas, and flue gas with high GEM levels (Carter, 2004; Fain et al., 2010; Jongman et al., 1995; Spuler et al., 2000; Tao et al., 2000). Microwave-induced plasmas (MIP)-CRDS with 20 Hz repetition rate and sensitivities that ranged from  $400$  to  $1841 \text{ ng m}^{-3}$  for 2 to 5 s were used for measurements of GEM in argon gas (Duan et al., 2005; Wang et al., 2005); and cavity-enhanced absorption spectroscopy (CEAS) with a sensitivity of  $66 \text{ ng m}^{-3}$  for 10 s ( $3\sigma$ ) was used for measurements of GEM in a static cell (Darby et al., 2013). As discussed, very few of these systems have been adapted for GEM concentration measurements under real-time, ambient air conditions.

## 3 Development of CRDS sensor for high-time-resolution measurements in ambient air

### 3.1 Wavelength locking and stabilization using an external Hg cell

Exact positioning and control of the laser wavelength is a critical requirement for replicable and reliable spectroscopic measurements. The output wavelength of the dye laser (tunable between 215 and 280 nm) is based on the mechanical position of a tuning grating, which supplies a relatively inaccurate measure of actual wavelength ( $\pm 0.03$  nm). This level of accuracy is insufficient to precisely position the laser wavelength onto the narrow GEM absorption line ( $0.005$  nm full width at half maximum, FWHM, at atmospheric pressure, Fig. 1a). To accurately control the laser wavelength relative to the wavelength of the GEM absorption line, we used an external Hg cell as a wavelength reference to control and position laser wavelength. A small fraction of the laser energy was deflected prior to the measurement cavity (Fig. 1b) using a fused silicate plate (ESCO Optics, Oak Ridge, NJ, USA). This beam was further split into two paths with near-equal beam power using a 1 : 1 UV beam splitter (Edmund Optics Inc., Barrington, NJ, USA): one path passed through the external Hg cell after which the transmitted power was quantified with a photodiode detector ( $\text{PD}_{\text{Hg}}$ ; DET10M, Thorlabs, Newton, NJ, USA); the second path without the Hg cell was used as reference, and its beam power was measured with a second photodiode detector ( $\text{PD}_{\text{ref}}$ ). Photodiode signals were routed into boxcar amplifiers (SR250, 2 ns Gated Integrator, Stanford Research Systems, Sunnyvale, CA, USA) where gate parameters were set to reduce the influence of background noise on the low-duty cycle signals. The resulting DC voltage signals were acquired with a data acquisition module (DAQ; National Instruments, Austin, TX, USA) at

50 Hz and routed to a LabVIEW program (National Instruments, Austin, TX, USA) for data processing. Using the ratio of these two photodiode signals provided a sensitive signal for positioning the laser wavelength. Note that the laser line width at 253.65 nm is  $\sim 0.9$  GHz (0.00019 nm), much narrower than the FWHM (0.005 nm) of the GEM absorption line.

We tested several external Hg cells made of 50 mm long, 8 mm diameter fused quartz tubes with two high quality fused silica windows attached at  $15^\circ$  angles (Fig. 1c, Thorlabs, Newton, NJ, USA). A 10 mm long stem that protrudes from the external Hg cell was filled with a small drop of liquid Hg; the vapor pressure of Hg (0.25 Pa at  $25^\circ\text{C}$ ; Schroeder et al., 1991) resulted in high vapor concentrations (and hence high absorption) of approximately  $2.1 \times 10^7$  ng  $\text{m}^{-3}$  at  $25^\circ\text{C}$  (Huber et al., 2006) inside the cells. Figure 1a shows the absorption spectra of three different Hg cells using the ratio of the two photodiode voltage signals ( $\text{PD}_{\text{Hg}}/\text{PD}_{\text{ref}}$ ) during wavelength scans across the GEM absorption spectrum. Low  $\text{PD}_{\text{Hg}}/\text{PD}_{\text{ref}}$  ratios reflect the strongest absorption of GEM when the laser wavelength matches the peak of the GEM absorption spectrum. The three cells include an Hg cell filled with metallic Hg at ambient pressure ( $\sim 80$  kPa within cell; green line); an Hg cell filled with metallic Hg under low pressure ( $1.33 \times 10^{-5}$  Pa within cell; blue line); and the spectrum of an Hg cell filled with an isotopically enriched, metallic  $^{200}\text{Hg}$  (94 % + isotopic purity) under low pressure ( $1.33 \times 10^{-5}$  Pa within cell; red line). In the low-pressure GEM spectrum (blue line), five of seven known stable Hg isotopes (Schroeder and Munthe, 1998; Spuler et al., 2000) can be seen as individual hyperfine structures, which are commonly observed when atmospheric pressure broadening is eliminated (Anderson et al., 2007; Spuler et al., 2000; Schweitzer, 1963). Differences between the external Hg cell at ambient pressure (green line) and low pressure (blue line) result from collisions of Hg atoms with air molecules, shortening their radiative lifetime or resulting in a phase shift and causing collision-induced/pressure broadening of the absorption line (Demtröder, 2003). The absorption spectrum of the  $^{200}\text{Hg}$  cell (red line) was much narrower than that of the “natural” metallic GEM and had a single, well-defined peak corresponding to absorption by the  $^{200}\text{Hg}$  isotope (the second most abundant stable Hg isotope with a mole fraction of 0.23; Spuler et al., 2000). The peak of the  $^{200}\text{Hg}$  absorption corresponded well to the peak of the ambient pressure GEM absorption (i.e., the peak that should be present in the measurement cavity when operated under ambient air conditions). Therefore, we used this  $^{200}\text{Hg}$  low-pressure cell to precisely position and control the laser wavelength during measurements.

Maintaining the laser wavelength on the peak absorption of the  $^{200}\text{Hg}$  cell was automated with a custom LabVIEW control program. A set of commands was implemented to continuously correct for slight drifts in laser wavelength (which are inherently caused by mechanical instabilities

due to temperature and other changes). The program minimized the  $\text{PD}_{\text{Hg}}/\text{PD}_{\text{Ref}}$  ratio by changing the laser wavelength in small increments (0.0002 nm) using a grating tuning element: if moving in one direction caused a decrease in  $\text{PD}_{\text{Hg}}/\text{PD}_{\text{ref}}$  ratios (i.e., moving toward the peak absorption), the program was set to continue changing wavelengths in that direction; if  $\text{PD}_{\text{Hg}}/\text{PD}_{\text{ref}}$  ratios increased, the program switched the direction to move the wavelength back toward the peak  $^{200}\text{Hg}$  absorption. A time average function was used to implement a 4 s moving average of the  $\text{PD}_{\text{Hg}}/\text{PD}_{\text{Ref}}$  ratio to avoid unnecessary wavelength changes due to noise. Using this approach, we successfully positioned and locked the laser wavelength on the  $^{200}\text{Hg}$  absorption line.

### 3.2 Implementation of differential absorption measurements

CRDS measures total extinction losses in the cavity, and, in order to separate GEM absorption ( $\alpha_{\text{Hg}}$ ) from other system losses, the sum of all other signal losses in the cavity must be determined ( $\alpha_{\text{BG}}$  and  $\alpha_{\text{M}}$ ; Eq. 1). Most spectroscopy techniques use differential absorption measurements to correct for such baseline losses; this can be achieved by consecutive measurement of spectral extinction losses with and without the compound of interest present (e.g., by removing (scrubbing) the compound of interest from the sample prior to a measurement) or employing measurements in two parallel extinction cells where the compound of interest is scrubbed from one sample stream (e.g., Model 205 Ozone analyzer, 2B Technologies, Boulder, CO, USA; or Model LI7000 infrared  $\text{CO}_2$  gas analyzers, LI-COR Inc., Lincoln, NE, USA).

We implemented differential extinction measurements using high-frequency wavelength tuning taking advantage of the uniquely narrow GEM absorption line. A piezoelectric tuning element (custom-supplied by Sirah) located in the dye laser allows for detuning of the laser wavelength (by  $\sim 0.003$  nm) from the original wavelength (i.e., peak GEM absorption of the external Hg cell). The piezoelectric tuning element allows for alternating laser wavelengths on a pulse-by-pulse basis (i.e., 50 Hz) from the peak GEM absorption line (called “online”) to an area directly adjacent (either to a higher or lower wavelength, called “offline”), thereby providing pairs of differential online and offline measurements at a 25 Hz repetition rate. To assure synchronization of the pulses emitted by the Nd:YAG laser and the piezoelectric tuning position, a piezo output signal triggers the lamp of the Nd:YAG pump laser to fire. GEM is uniquely suited for such differential online and offline extinction measurements due to its very narrow absorption line (FWHM 0.005 nm) as it is the only tropospheric constituent that occurs in elemental form and for which the transition to an excited state ( $6^1\text{S}_0$  to  $6^3\text{P}_1$ ) is not spread across a large number of rotational and vibrational transitions as it is for molecular constituents (Spuler et al., 2000; Edner et al., 1989). Detuning of the laser wavelength by such a small increment should, therefore, ensure

that the system is only sensitive to GEM absorption while the broader absorption lines of other compounds (such as  $O_3$  or  $SO_2$ ) should remain unchanged by such small wavelength shifts.

The final wavelength conversion of the laser system occurs in a frequency conversion unit (FCU) containing a barium borate (BBO) frequency doubling crystal that converts the fundamental dye laser wavelength from 507.3 nm to its second harmonic of 253.65 nm. After the differential measurement setup was finalized, we noticed that the frequency conversion efficiency of online and offline measurements changed through time, which caused large drifts in differential extinction measurements as online and offline measurements were affected differently by these drifts. As a result, we had to implement a mechanism to continuously adjust the FCU position in order to maintain equal wavelength conversion efficiencies for both wavelengths of the differential measurements. We implemented a function in our LabVIEW control program to adjust the FCU position to reduce the difference in signal power to less than about 2% of the signal voltage between the online and offline signals measured by the  $PD_{Ref}$ .

### 3.3 Signal acquisition, automated signal processing, and calculation of GEM concentrations

In our system, energy from laser pulses in the cavity leaks out through the back mirror of the cavity where signals are captured by a photomultiplier tube (PMT; Model H6780; Hamamatsu, Japan). A CompuScope data acquisition card (CompuScope 12100, GaGe, Lockport, Illinois, USA) is used to digitize the analog signal, which is then processed in real time by our custom LabVIEW CRDS program (Fig. 2a). The exponential ring-down of each laser pulse (at 50 Hz pulse repetition rate) is quantified by 200 measurement points recorded with an acquisition rate of  $1\text{ MS s}^{-1}$ . Each acquisition is initiated by the laser Q-switch trigger signal synchronizing signal acquisition with laser pulses. Since the first few data points of each ring-down signal showed non-exponential decay patterns, possibly caused by an incomplete match between transverse beam and cavity modes, we eliminated the first 15 points of each ring-down. The program then performed an exponential fit to each decay using the non-linear Levenberg–Marquardt method at 50 Hz (Press et al., 1986). The three fitting parameters (initial, baseline signal, and extinction coefficient,  $\alpha$ ) were exported and saved to a data file.

Because of the high-frequency differential tuning/detuning of the laser wavelength during measurements, online extinction measurements needed to be separated from offline measurements; this was done by reading the position of the piezoelectric tuning element (a sinusoidal analog wave form with the apex representing the online position and the trough representing the offline signal) using the second channel of the CompuScope acquisition card. Both extinction measurements were continuously graphed during operation so that

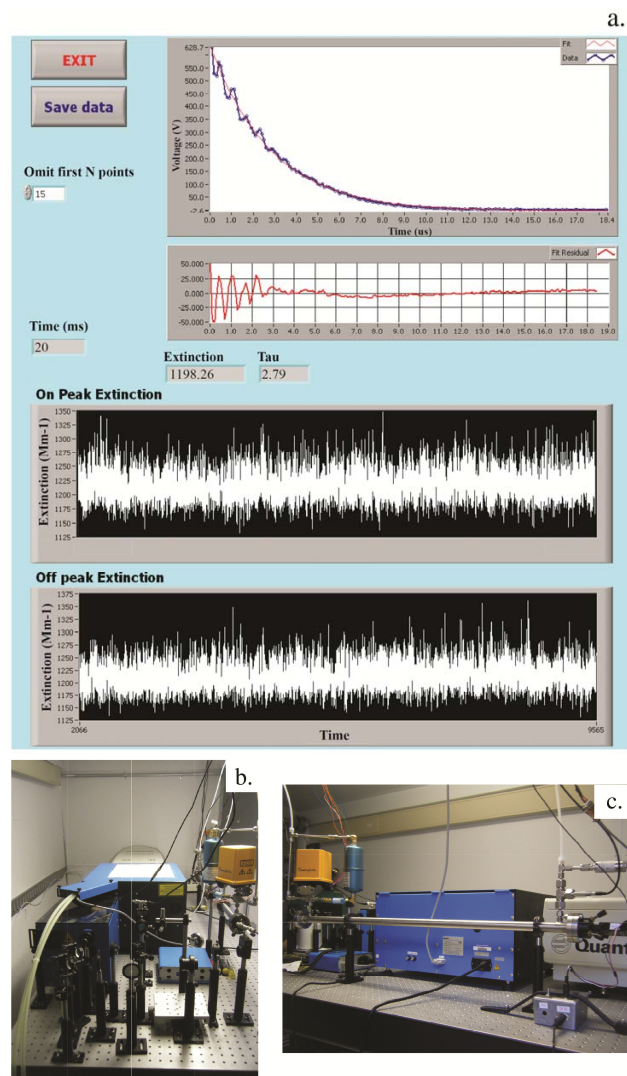


**Fig. 2.** (a) LabVIEW interface with raw ring-down and residual signal graph. The first 15 points are omitted from the ring-down graph. Both online and offline extinction graphs are visible during operation to visualize separation of the two signals. The interface also displays the extinction and ring-down time constants ( $\tau$ ) at 50 Hz. (b) Laser setup on optical table inside the mobile trailer. (c) CRDS cavity with laser in the background inside the trailer.

differential measurements were visible on a screen in real time (Fig. 2a).

For ambient air measurements, differential extinction – corresponding to absorption by GEM – is calculated as the difference between online and offline extinction measurements. The measured differential extinction is adjusted for a measured Hg-free air offset. In addition, changes in environmental conditions (e.g., temperature, pressure, and relative humidity) as well as laser and system variables (e.g., absolute system extinction, wavelength position, and frequency conversion efficiency) influenced differential CRDS measurements; these factors are addressed by using a multi-linear

regression correction. To calculate GEM, a conversion factor between differential extinction and GEM (number of  $\text{Mm}^{-1}$  per  $\text{ng Hg m}^{-3}$ ) is calculated each day by comparison of measurements to a Tekran 2537 analyzer across corresponding 2.5 min measurement intervals.

With these setup changes, the CRDS sensor has been run automatically and continuously for measurements in the field for up to 11 h (about 1 million differential measurements) on multiple consecutive days. Flash lamps must be changed every 30 million shots (about seven days of continuous run time), and dye must be changed every two weeks with heavy use (5–8 h per day, 5 days per week), maintenance that can be done easily by a trained technician.

### 3.4 Other system modifications to conduct field measurements

Several modifications to the system were required for field deployment. First, the optical components of the system were mounted on a mobile optical table to ensure stability of optical paths (Fig. 2b and c) and to allow for the system to be moved into a  $4.3 \times 2.4$  m air-conditioned mobile trailer. Second, an external chiller was connected to allow for water cooling of the Nd:YAG laser. Third, the measurement cavity was thermally insulated using a foam box to further minimize temperature drifts in and around the measurement cavity. And fourth, the sample inlet was modified to reduce particulate matter and  $\text{O}_3$  interferences.

Despite implementation of differential measurements, our system still showed  $\text{O}_3$  interferences during ambient air measurements (see Sect. 4.3). Therefore, we configured our inlet setup to remove  $\text{O}_3$  in the sampling stream. Efficient removal of  $\text{O}_3$  from the sample proved difficult since most known  $\text{O}_3$  scrubbers also remove at least some GEM, which would invalidate measurements. We tested several methods of  $\text{O}_3$  scrubbing and characterized their efficiency for  $\text{O}_3$  and GEM removal (Table 2). For example, copper oxide (CuO) coated copper coils proved highly efficient at removing  $\text{O}_3$  from a sample stream, but unfortunately this method also removed a significant fraction of GEM. After extensive testing, we found that thermal decomposition of  $\text{O}_3$  at  $500^\circ\text{C}$  reduced  $\text{O}_3$  concentrations below the detection limit (d.l.) of our  $\text{O}_3$  analyzer ( $> 1.0$  ppbv; 2B Technologies, 2011) while it did not affect GEM concentrations.

Sample inlets to the trailer consisted of 4.76 mm ID Teflon<sup>®</sup> tubing and  $0.2 \mu\text{m}$  pore size, 47 mm diameter Teflon filters and a 5 m length of unheated Teflon line; unheated Teflon filters and lines generally do not transmit RGM or PHg (Brunke et al., 2010; Moore et al., 2013), so only GEM should transmit through this inlet. Air flow was directed through two ovens to thermally decompose  $\text{O}_3$ ; this was done by using the heating ovens of a Tekran speciation unit (Model 1130 and 1135, Tekran Inc., Toronto, Canada); flow was routed through a set of cleaned glassware (annular denuder and particulate trap glassware, not coated and without

**Table 2.** Methods for removing  $\text{O}_3$ .

Removal type	$\text{O}_3$ (ppb)	$\text{O}_3$ removal (%)	GEM removal (%)
Ambient Air	$39.4 \pm 10$		
Tekran charcoal filter	< d.l.	> 99	100
KI denuder	0.8	> 95	~ 50
CuO + Cu coil	2.1	90–95	~ 50
$\text{NaS}_2\text{O}_3$ coated denuder	2.8	90–95	0
$\text{NaS}_2\text{O}_3$ packed column	< d.l.	> 99	< 5
Thermal $\text{O}_3$ destruction at $500^\circ\text{C}$ with high surface area (annular denuders and glass tubes filled with quartz chips)	< d.l.	> 99	0

a filter, but packed with quartz chips to increase surface area) heated to  $500^\circ\text{C}$ . Flow through the cavity was set to rates variable up to  $10 \text{ L min}^{-1}$  using a flowmeter (Aalborg, Orangeburg, NY, USA) and external pump, which resulted in a sample transmission time from the end of the sample line to the cavity of about 2 s.

## 4 CRDS measurements and GEM spike additions in Hg-free and ambient air

We performed measurements of GEM with various GEM spike additions using GEM permeation sources both in Hg-free air (i.e., air filtered by a charcoal filter; Zero Air Filter Model 30-25150-00, Tekran Inc., Toronto, Canada) and ambient air. Two methods of GEM addition were used: first, stable GEM concentrations were created for 10 min by a combination of flow controllers that mixed air from an Hg permeation tube (HE-SR 1.7CM; VICI Metronics Inc., Poughkeepsie, NY, USA) in a temperature-controlled water bath with Hg-free air (Model 1100, Tekran Inc., Toronto, Canada) to generate GEM concentrations ranging from 0 to  $127 \text{ ng m}^{-3}$ ; a second method of GEM addition directly injected GEM from a mercury vapor calibration unit (Model 2505, Tekran Inc., Toronto, Canada) into Hg-free air supplied to the measurement cavity. GEM was injected using an injection syringe (Digital Syringe 07873, Hamilton Co., Reno, NV, USA), thereby generating short pulses of GEM concentrations ranging from 0 to  $20 \text{ ng m}^{-3}$ . At least 10 min separated each GEM spike addition to allow for concentrations to decline to the baseline (Hg-free air or ambient air concentrations) prior to the next injection. The following sections describe the GEM measurements in Hg-free and ambient air.

### 4.1 GEM measurements in Hg-free air

Figure 3 shows two sets of calibrations performed in Hg-free air in July 2011 (Fig. 3a) and July 2012 (Fig. 3b) with GEM concentration spikes ranging from  $0 \text{ ng m}^{-3}$  to  $127 \text{ ng m}^{-3}$ . GEM spikes are shown as GEM enhancements

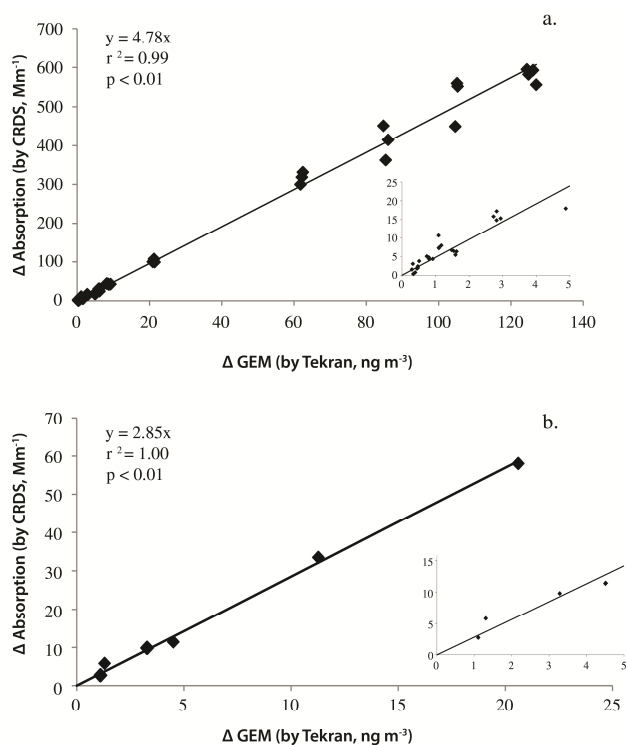


**Fig. 3.** (a) Scatterplots between Tekran and CRDS measurements during a calibration in Hg-free air performed 14 July 2011. (b) same as (a) for measurements on 19 July 2012. The insets for each graph show data in the range of 0 to 5  $\text{ng m}^{-3}$  only.

(i.e., difference in GEM during spikes and a period immediately after the spikes;  $\Delta$  GEM); similarly, the response of the CRDS system to a GEM spike is calculated as the differential CRDS extinction during the spike minus that immediately following the spikes (i.e.,  $\Delta$  Absorption). Both sets of calibrations showed highly linear relationships (Fig. 3a:  $r^2 = 0.99$ ; Fig. 3b:  $r^2 > 0.99$ ) between the spike response of the CRDS system ( $\Delta$  Absorption) and that of the Tekran instrument ( $\Delta$  GEM). This result is in agreement with previous laboratory tests showing high linearity between CRDS GEM absorption measurements and Tekran GEM measurements ( $r^2 > 0.99$ ; Faïn et al., 2010). The highly linear relationships suggest that both systems, although based on different detection mechanisms, were highly linear across concentration ranges of 0 to 573  $\text{ng m}^{-3}$  without any saturation artifacts (see also Faïn et al., 2010).

We observed differences in slopes between measured CRDS differential extinction and Tekran GEM concentrations among various sets of measurements. Slopes between CRDS differential extinction and Tekran GEM concentrations represent a conversion factor linking GEM absorption (units of  $\text{Mm}^{-1}$ ) to concentration (units of  $\text{ng m}^{-3}$ ). Conversion factors in Fig. 3 were 4.85  $\text{Mm}^{-1}$  per  $\text{ng Hg m}^{-3}$  in July 2011 and 2.85  $\text{Mm}^{-1}$  per  $\text{ng Hg m}^{-3}$  in July 2012. Hence, conversion factors differed between the

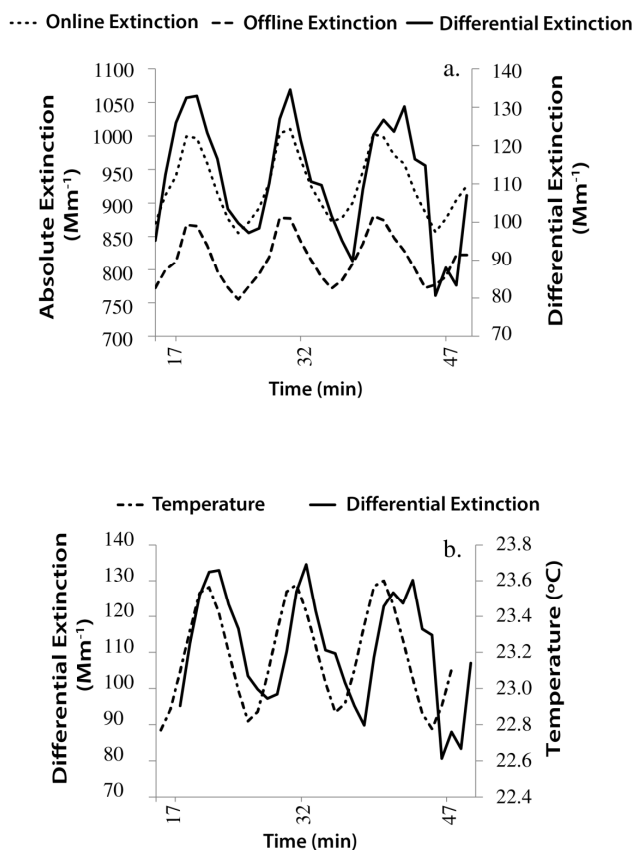


**Fig. 4.** (a) Online and offline absolute extinction signals and differential extinction as a function of time measured during an afternoon where we noticed significant temperature fluctuations (1 min averaging time). (b) Differential extinction and corresponding temperature fluctuations during that afternoon (1 min averaging time).

measurements, as well as from a previous conversion factor obtained from the laboratory prototype (6.03  $\text{Mm}^{-1}$  per  $\text{ng m}^{-3}$ ; Faïn et al., 2010). It is unclear why conversion factors changed, but possible reasons include major changes in the system (e.g., use of different mirrors with potentially different reflectivity), changes in operation (use of differential extinction measurements), and changes in signal acquisition and analysis. An additional factor may be a change in mirror reflectivity due to changes in temperature and humidity. To account for different conversion factors, we calibrated our system daily by establishing specific conversion factors for each day of measurements using GEM spike additions or by comparison of data to a Tekran 2537 analyzer. As mentioned in Faïn et al. (2010), a literature absorption coefficient was not used as it did not fit our observed conversion coefficient, although the reasons for this are unclear.

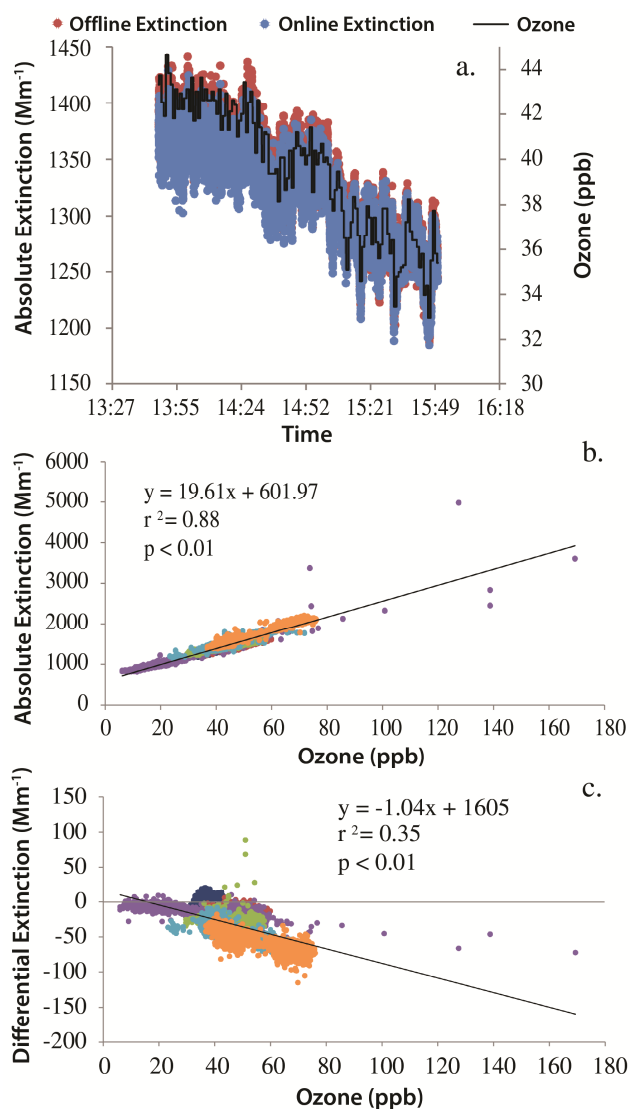


**Fig. 5.** Relationships between CRDS extinction measurements and O<sub>3</sub> concentrations: **(a)** CRDS extinction measurements on 29 February 2011 for two hours that show how extinction changes as a function of ambient O<sub>3</sub> concentrations. **(b)** Linear relationship between CRDS absolute extinction measurements and O<sub>3</sub> concentration during six days of measurements. **(c)** Same as **(b)** but showing differential extinction also affected by O<sub>3</sub> concentrations.

#### 4.2 GEM measurements in ambient air – temperature interferences

Although inlet air temperatures were stabilized by the external ovens of the inlet systems and the sensor was inside an air-conditioned trailer, we detected small temperature fluctuations (mainly related to the on-and-off cycles of the air conditioning) inside the cavity during ambient air measurements. Figure 4a shows how a cyclical fluctuation of temperature affected online and offline extinction during measurements; most importantly, however, the temperature fluctuations also

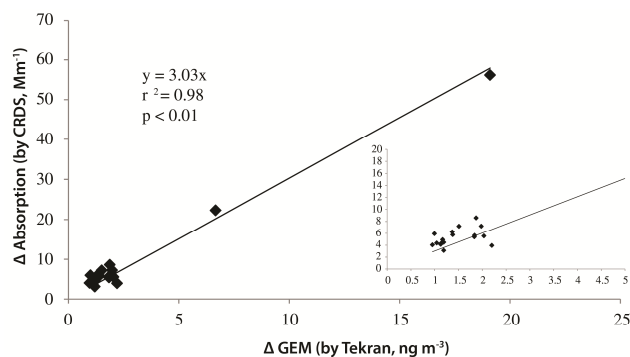


**Fig. 6.** Scatterplots between Tekran and CRDS measurements during a calibration in ambient air performed 19 July 2012. The inset shows data from 0 to 5 ng m<sup>-3</sup>.

affected the differential extinction as shown in Fig. 4b. A slight delay of the cavity response to temperature changes may be caused by temperature-sensitive element(s) of the cavity showing a delayed response to temperature changes, or by the fact that the temperature measurements were taken at the cavity outlet port rather than inside the cavity. To address these temperature effects, we constructed a foam enclosure that covered the entire measurement cavity and reduced the temperature fluctuations to  $< 1^\circ\text{C}$  during measurements. The foam enclosure greatly reduced temperature fluctuations, although it did not completely eliminate them. The remaining effect of temperature on measured extinction was corrected using a linear regression function (Sect. 3.3).

#### 4.3 GEM measurements in ambient air – ozone interference

Between February and June 2012, we conducted 20 days of CRDS measurements in ambient air in Reno, Nevada, and compared measurements with the CRDS system (2.5 min averaged data) to GEM concentrations measured by a Tekran 2537 (averaged across the same time intervals) in the same location. Measurements generally lasted from  $\sim 3$  to 6 h; average ambient air GEM concentration during this time was  $1.5 \text{ ng m}^{-3}$  (with a range of 0.85 to  $2.05 \text{ ng m}^{-3}$ ). Considerable O<sub>3</sub> concentrations were present in ambient air in Reno (between 20 to 50 ppb), and during the first six days (before the inlet system was configured to thermally decompose O<sub>3</sub>), measurements showed strong interferences by O<sub>3</sub> (Fig. 5a, b, and c). While we expected the absolute CRDS extinction to be highly sensitive to O<sub>3</sub> due to its strong absorption at 254 nm, the use of differential extinction measurements in theory should preclude sensitivity to O<sub>3</sub> (see Sect. 3.2).

Unexpectedly, we found that the presence of O<sub>3</sub> concentrations still caused significant interference during measurements as evident in inverse relationships between O<sub>3</sub> concentrations and differential extinction (Fig. 5c). Possible reasons for this interference are that high ( $> 10 \text{ ppb}$ ) O<sub>3</sub> concentrations that cause strong extinction losses ( $\sim 2000 \text{ Mm}^{-1}$ )

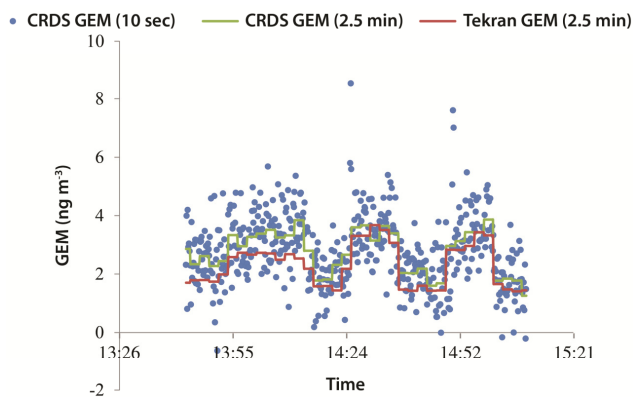


**Fig. 7.** Ambient air measurement for 1.5 h and comparisons of GEM measured by the CRDS system and a Tekran 2537B Hg analyzer (in  $\text{ng m}^{-3}$ ) with 1–2  $\text{ng m}^{-3}$  GEM spike additions.

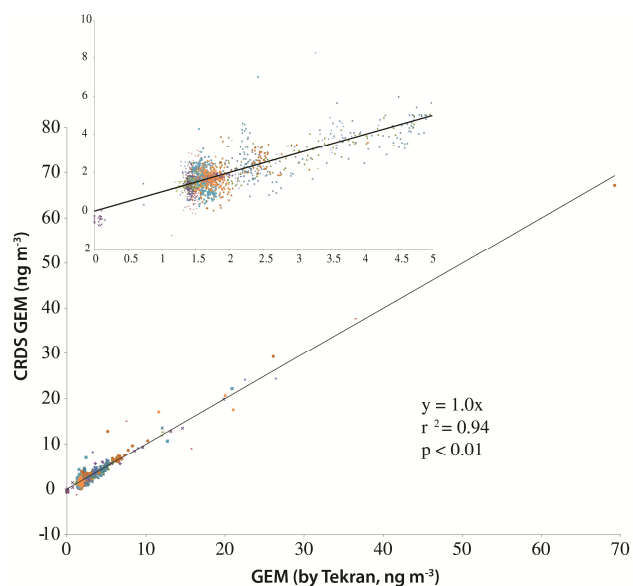


**Fig. 8.** Comparison of real-time, continuous concentration measurements between the CRDS system (calculated GEM concentrations from differential extinction in  $\text{ng m}^{-3}$ ) and a commercially available GEM sensor (GEM concentrations in  $\text{ng m}^{-3}$ ) that operates with a 2.5 min time resolution. The graph shows the whole dataset of measurements made in ambient air with spikes at various concentrations of GEM using a GEM permeation source. Different symbols and colors represent the 10 days of testing. Inset shows data between 0 and 5  $\text{ng m}^{-3}$ .

may reduce the CRDS sensitivity or affect its exponential decay function. At 254 nm, GEM has a higher absorption cross section than  $\text{O}_3$ ,  $3.3 \times 10^{-14} \text{ cm}^2 \text{ molecule}^{-1}$  (Jongma et al., 1995; Edner et al., 1989; Spuler et al., 2000) versus  $1.2 \times 10^{-17} \text{ cm}^2 \text{ molecule}^{-1}$  (Griggs, 1968; Inn and Tanaka, 1953; Molina and Molina, 1986; Mauersberger et al., 1986), but the absorption by  $\text{O}_3$  in ambient air is still much higher than that of GEM due to the higher  $\text{O}_3$  concentrations ( $\sim$  five orders of magnitude). A possible way to account for  $\text{O}_3$

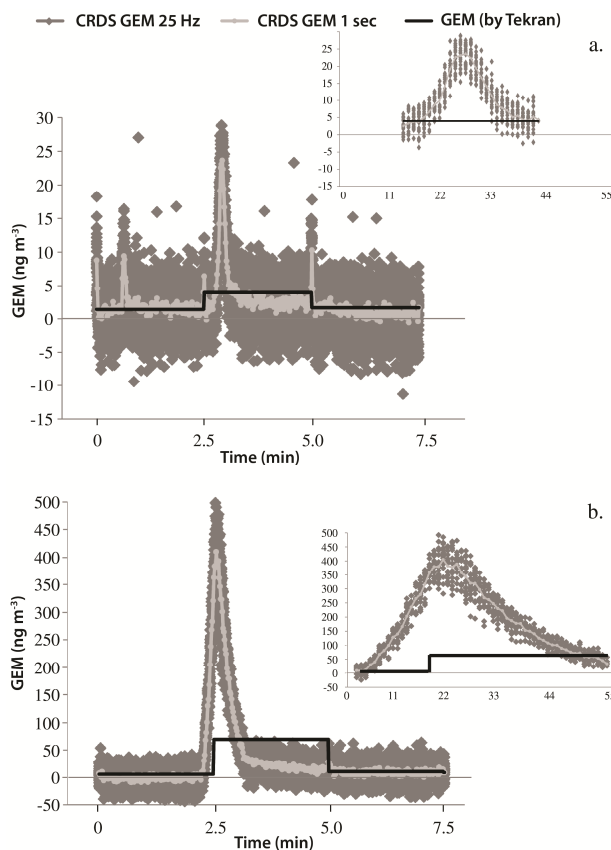


**Fig. 9.** High-resolution CRDS measurements on 15 June 2012 with short GEM spike additions to ambient air, and comparison to measurements using a Tekran Hg analyzer. CRDS measurements are shown at 25 Hz and 1 s time resolutions, while Tekran measurements are shown at 2.5 min resolution. **(a)** 4  $\text{ng m}^{-3}$  spike, **(b)** 70  $\text{ng m}^{-3}$  spike. Insets for both panels include only the spike area.

interferences would be to use the linear regression equation for correction, but the predictive value of the regression ( $r^2 = 0.35$ ) is relatively low. Instead, we opted to remove  $\text{O}_3$  from the sample stream during measurements using thermal decomposition as described in Sect. 3.4.

#### 4.4 GEM measurements in ambient air stripped of $\text{O}_3$

With the inlet configuration that removes  $\text{O}_3$ , we performed measurements using GEM spike additions in the range of 0.9 to 19.1  $\text{ng m}^{-3}$  added to urban background air (average GEM concentration of  $\sim 1.5 \text{ ng m}^{-3}$ ; Fig. 6). The coefficient of determination,  $r^2$ , between CRDS absorption measurements and GEM measured by a Tekran analyzer was similar ( $r^2 > 0.99$ ) to that of spike calibrations in Hg-free air (Fig. 3;  $r^2 = 0.99$ , July 2011, and  $> 0.99$ , July 2012). We calculated a standard deviation ( $\sigma$ ) of the CRDS GEM absorption measurements during periods when ambient GEM concentrations were relatively stable (between

1.3 and 1.7 ng m<sup>-3</sup>). The standard deviation of calculated GEM concentrations ( $N = 79\,325$ , or 53 min of 25 Hz observations) was  $\pm 10.2$  ng m<sup>-3</sup>. Based on this variability, we estimated a system sensitivity for GEM in ambient air as 30.6 ng m<sup>-3</sup> ( $3\sigma$ ) at 25 Hz. Using time averaging of observations (i.e.,  $\sigma/\sqrt{n}$ ), our estimated system sensitivity for ambient air measurements was approximately 6.1 ng m<sup>-3</sup> at 1 s time resolution, 1.9 ng m<sup>-3</sup> at 10 s time resolution, 0.5 ng m<sup>-3</sup> at 2.5 min time resolution, and 0.35 ng m<sup>-3</sup> at 5 min time resolution. This sensitivity calculation assumed fully stable GEM concentrations during the measurement times and all variability attributable to the CRDS system, which likely is not the case; hence, calculated sensitivity presents a conservative, upper limit. In Fig. 7, we show a sequence of 1.5 h of measurements in ambient air with small 1–2 ng m<sup>-3</sup> GEM spike additions demonstrating good agreement between the CRDS measurements and the Tekran analyzer at ambient and near-ambient GEM concentrations.

In Fig. 8, we show a longer term dataset of GEM concentration measurements with occasional GEM spike additions performed during 10 days of measurements. This dataset shows larger differences between CRDS measurements and corresponding Tekran GEM measurements compared to results of spike additions shown in Figs. 3 and 6. Statistical analysis showed that differences between the CRDS and Tekran measurements for a total of 73 h of measurements were within 0.1 ng m<sup>-3</sup> for 12 % of the data, within 0.2 ng m<sup>-3</sup> for 23 % of the data, within 0.5 ng m<sup>-3</sup> for 43 % of the data, and within 1.0 ng m<sup>-3</sup> for 63 % of the data. The increased variability observed during multiple days of observations is attributed to instability of the CRDS sensor through time. To confirm this, we analyzed the data using Allan variance, a method that summarizes variability in temporal data as a function of the time integration period (Werle et al., 1993). We found that the Allan variance decreased with time of averaging up to a time integration step of 40 s; the decrease in variance was close to a slope of  $-1$ , a pattern that is generally attributed to a decrease in white noise due to temporal averaging of data (Werle et al., 1993). For a time-averaging period greater than 40 s, however, the Allan variance in CRDS data starts to increase substantially. These patterns indicate an increase in random drifts in system noise after 40 s time, and they suggest that the best temporal averaging time for measured CRDS data is in the range of 40 s.

#### 4.5 High-time-resolution patterns during GEM spike additions

Despite challenges in longer term system stability, a key advantage of the CRDS measurements includes high temporal resolution of 25 Hz. Figure 9a and b show two examples when GEM spikes were added to ambient air (4 and 70 ng m<sup>-3</sup>, respectively) by means of short syringe injections. The graphs show that slow-response Tekran measurements (i.e., 2.5 min time resolution) largely missed the shape

and magnitude of these GEM spikes. For example, Tekran measurements showed a spike concentration of 3.9 ng m<sup>-3</sup> during 2.5 min for a spike that actually reached as high as 28 ng m<sup>-3</sup> when measured at high temporal resolution with the CRDS system (Fig. 9a). The figure also shows that the resulting GEM spike was of very short duration (approximately 26 s). Similarly, in Fig. 9b, Tekran measurements show a spike of 69 ng m<sup>-3</sup> during 2.5 min for a spike that actually reached as high as 410 ng m<sup>-3</sup> and lasted for approximately 55 s. This spike showed a very steep increase at the beginning (about 19 s) and a slightly longer decrease time for the spike to be fully transmitted through the inlet and concentrations to reach background GEM levels (about 36 s).

The high temporal resolution possible with CRDS observations can make significant contributions to characterizing atmospheric GEM patterns related to pollution episodes as well as surface–atmosphere exchange fluxes by means of the eddy covariance technique (e.g. over Hg-enriched sites; Pierce et al., 2013). A further application of this sensor is in laboratory investigations to study fast interactions of GEM concentrations with additions of atmospheric oxidants to assess reaction kinetics as currently performed in our laboratory (Darby et al., 2013; Venables et al., 2013). To our knowledge, results reported here represent the first comparison of GEM measurements by a CRDS sensor with an independent, commercially available sensor under ambient air conditions using high time resolution, continuous measurements. We showed that CRDS allows for characterization of GEM concentrations in the ambient concentration range; but across longer time periods, ambient air CRDS measurements show increased variability. Although sensitivity and stability of the system currently do not match those of commercially available sensors, the sensitivity is improved compared to previous CRDS sensors. The main advantage of CRDS GEM detection is high-time-resolution measurements that allow for characterization of short spikes and fast concentration fluctuations that are not possible with slow-response sensors.

*Acknowledgements.* We would like to thank Nicholas Nussbaum for software development, Rick Purcell for technical assistance and engineering, Luke Arnone for technical help, Roger Kreidberg for editorial assistance, Mike Crumb for technical laser assistance, and the facilities crew at the Desert Research Institute for assistance with the mobile trailer setup. This system development and study were supported by a US National Science Foundation Major Instrumentation (NSF MRI) grant (Award Number: 0923485) and an NSF grant from the Division of Atmospheric and Geospace Sciences (Award Number: 1101924).

Edited by: P. Werle

## References

- Anderson, T. N., Magnuson, J. K., and Lucht, R. P.: Diode-laser-based sensor for ultraviolet absorption measurements of atomic mercury, *Appl. Phys. B*, 87, 341–353, doi:10.1007/s00340-007-2604-z, 2007.
- Arya, S. P.: Introduction to Micrometeorology, Academic Press, San Diego, 2001.
- Atkinson, D. B.: Solving chemical problems of environmental importance using cavity ring-down spectroscopy, *Analyst*, 128, 117–125, 2003.
- Bauer, D., Campuzano-Jost, P., and Hynes, A. J.: Rapid, ultra-sensitive detection of gas phase elemental mercury under atmospheric conditions using sequential two-photon laser induced fluorescence, *J. Environ. Monitor.*, 4, 339–343, 2002.
- Bauer, D., D’Ottone, L., Campuzano-Jost, P., and Hynes, A. J.: Gas phase elemental mercury: a comparison of LIF detection techniques and study of the kinetics of reaction with the hydroxyl radical, *J. Photochem. Photobiol. A*, 157, 247–256, 2003.
- Brunke, E.-G., Labuschagne, C., Ebinghaus, R., Kock, H. H., and Slemr, F.: Gaseous elemental mercury depletion events observed at Cape Point during 2007–2008, *Atmos. Chem. Phys.*, 10, 1121–1131, doi:10.5194/acp-10-1121-2010, 2010.
- Carter, C. C.: A Cavity Ring-Down Spectroscopy Mercury Continuous Emission Monitor, Sensor Research and Development Corporation, Orono, Maine 04473, 118 pp., 2004.
- Clevenger, W. L., Smith, B. W., and Winefordner, J. D.: Trace Determination of Mercury: A Review, *Crc. Cr. Rev. Anal. Chem.*, 27, 1–26, doi:10.1080/10408349708050578, 1997.
- Darby, S. B., Smith, P. D., and Venables, D. S.: Cavity-enhanced absorption using an atomic line source: application to deep-UV measurements, *Analyst*, 137, 2318–2321, 2012.
- Darby, S., Pierce, A., Moore, C., Moosmüller, H., Venables, D., and Obrist, D.: An atmospheric simulation chamber study of the bromine-initiated oxidation of mercury at a range of temperatures, International Conference on Mercury as a Global Pollutant, Edinburgh, Scotland, accepted presentation, 2013.
- Demtröder, W.: Laser Spectroscopy: basic concepts and instrumentation, Springer, Verlag, Berlin, Heidelberg, New York, 2003.
- Duan, Y. X., Wang, C. J., Scherrer, S. T., and Winstead, C. B.: Development of alternative plasma sources for cavity ring-down measurements of mercury, *Anal. Chem.*, 77, 4883–4889, doi:10.1021/ac050704x, 2005.
- Ebinghaus, R., Jennings, S. G., Schroeder, W. H., Berg, T., Donaghy, T., Guentzel, J., Kenny, C., Kock, H. H., Kvietskus, K., Landing, W., Muhleck, T., Munthe, J., Prestbo, E. M., Schneeberger, D., Slemr, F., Sommar, J., Urba, A., Wallschlager, D., and Xiao, Z.: International field intercomparison measurements of atmospheric mercury species at Mace Head, Ireland, *Atmos. Environ.*, 33, 3063–3073, 1999.
- Edner, H., Faris, G. W., Sunesson, A., and Svanberg, S.: Atmospheric atomic mercury monitoring using differential absorption lidar techniques, *Appl. Optics*, 28, 921–930, 1989.
- Faïn, X., Moosmüller, H., and Obrist, D.: Toward real-time measurement of atmospheric mercury concentrations using cavity ring-down spectroscopy, *Atmos. Chem. Phys.*, 10, 2879–2892, doi:10.5194/acp-10-2879-2010, 2010.
- Fitzgerald, W. F., Engstrom, D. R., Mason, R. P., and Nater, E. A.: The Case for Atmospheric Mercury Contamination in Remote Areas, *Environ. Sci. Technol.*, 32, 1–7, doi:10.1021/es970284w, 1998.
- Griggs, M.: Absorption Coefficients of Ozone in the Ultraviolet and Visible Regions, *J. Chem. Phys.*, 49, 857–859, 1968.
- Huber, M. L., Laesecke, A., and Friend, D. G.: Correlation for the Vapor Pressure of Mercury, *Ind. Eng. Chem. Res.*, 45, 7351–7361, doi:10.1021/ie060560s, 2006.
- Inn, E. C. Y. and Tanaka, Y.: Absorption Coefficient of Ozone in the Ultraviolet and Visible Regions, *J. Opt. Soc. Am.*, 43, 870–872, 1953.
- Jongma, R. T., Boogaarts, M. G. H., Holleman, I., and Meijer, G.: Trace Gas-Detection with Cavity Ring down Spectroscopy, *Rev. Sci. Instrum.*, 66, 2821–2828, 1995.
- Lamborg, C. H., Fitzgerald, W. F., O’Donnell, J., and Torgersen, T.: A non-steady-state compartmental model of global-scale mercury biogeochemistry with interhemispheric atmospheric gradients, *Geochim. Cosmochim. Ac.*, 66, 1105–1118, 2002.
- Landis, M. S., Stevens, R. K., Schaedlich, F., and Prestbo, E. M.: Development and Characterization of an Annular Denuder Methodology for the Measurement of Divalent Inorganic Reactive Gaseous Mercury in Ambient Air, *Environ. Sci. Technol.*, 36, 3000–3009, doi:10.1021/es015887t, 2002.
- Lindberg, S., Bullock, R., Ebinghaus, R., Engstrom, D., Xinbin, F., Fitzgerald, W., Pirrone, N., Prestbo, E., and Seigneur, C.: A Synthesis of Progress and Uncertainties in Attributing the Sources of Mercury in Deposition, *AMBIO – A Journal of the Human Environment*, 36, 19–32, 2007.
- Lyman, S. N., Jaffe, D. A., and Gustin, M. S.: Release of mercury halides from KCl denuders in the presence of ozone, *Atmos. Chem. Phys.*, 10, 8197–8204, doi:10.5194/acp-10-8197-2010, 2010.
- Mauersberger, K., Barnes, J., Hanson, D., and Morton, J.: Measurement of the ozone absorption cross section at the 253.7 nm mercury line, *Geophys. Res. Lett.*, 13, 671–673, doi:10.1029/GL013i007p00671, 1986.
- Molina, L. T. and Molina, M. J.: Absolute Absorption Cross Sections of Ozone in the 185- to 350-nm Wavelength Range, *J. Geophys. Res.*, 91, 14501–14508, doi:10.1029/JD091iD13p14501, 1986.
- Moore, C. W., Obrist, D., and Luria, M.: Atmospheric mercury depletion events at the Dead Sea: Spatial and temporal aspects, *Atmos. Environ.*, 69, 231–239, doi:10.1016/j.atmosenv.2012.12.020, 2013.
- Moosmüller, H., Varma, R., and Arnott, W.: Cavity Ring-Down and Cavity-Enhanced Detection Techniques for the Measurement of Aerosol Extinction, *Aerosol Sci. Tech.*, 39, 30–39, 2005.
- Munthe, J., Wängberg, I., Pirrone, N., Iverfeldt, Å., Ferrara, R., Ebinghaus, R., Feng, X., Gårdfeldt, K., Keeler, G., Lanzillotta, E., Lindberg, S. E., Lu, J., Mamane, Y., Prestbo, E., Schmolke, S., Schroeder, W. H., Sommar, J., Sprovieri, F., Stevens, R. K., Stratton, W., Tuncel, G., and Urba, A.: Intercomparison of methods for sampling and analysis of atmospheric mercury species, *Atmos. Environ.*, 35, 3007–3017, doi:10.1016/S1352-2310(01)00104-2, 2001.
- OhioLumex: RA-915+ Portable Mercury Vapor Analyzer, available at: [http://www.ohiolumex.com/products/ra915\\_mercury\\_analyzer.php](http://www.ohiolumex.com/products/ra915_mercury_analyzer.php) (last access: 8 February 12), 2012.
- Pandey, S. K., Kim, K.-H., and Brown, R. J. C.: Measurement techniques for mercury species in ambient air, *TrAC Trend. Anal. Chem.*, 30, 899–917, doi:10.1016/j.trac.2011.01.017, 2011.

- Pierce, A., Obrist, D., Moore, C., and Wohlfahrt, G.: A cavity ring-down spectroscopy sensor for measurements of gaseous elemental mercury: Eddy covariance flux measurements over natural and Hg-enriched soils, in preparation, 2013.
- Press, W. H., Flannery, B. P., Teukolsky, S. A., and Wetterling, W. T.: Numerical Recipes: The art of scientific computing, 3rd Edn., Cambridge University Press, Cambridge, New York, 1986.
- Rothenberg, S. E., Mckee, L., Gilbreath, A., Yee, D., Connor, M., and Fu, X. W.: Evidence for short-range transport of atmospheric mercury to a rural, inland site, *Atmos Environ*, 44, 1263–1273, doi:10.1016/j.atmosenv.2009.12.032, 2010.
- Schroeder, W. H. and Munthe, J.: Atmospheric mercury – An overview, *Atmos. Environ.*, 32, 809–822, 1998.
- Schroeder, W. H., Yarwood, G., and Niki, H.: Transformation processes involving mercury species in the atmosphere – results from a literature survey, *Water Air Soil Poll.*, 56, 653–666, doi:10.1007/bf00342307, 1991.
- Schroeder, W. H., Keeler, G., Kock, H., Roussel, P., Schneeberger, D., and Schaedlich, F.: International field intercomparison of atmospheric mercury measurement methods, *Water Air Soil Poll.*, 80, 611–620, 1995.
- Schweitzer, J. W. G.: Hyperfine Structure and Isotope Shifts in the 2537-Å Line of Mercury by a New Interferometric Method, *J. Opt. Soc. Am.*, 53, 1055–1071, 1963.
- Shia, R.-L., Seigneur, C., Pai, P., Ko, M., and Sze, N. D.: Global simulation of atmospheric mercury concentrations and deposition fluxes, *J. Geophys. Res.*, 104, 23747–23760, doi:10.1029/1999jd900354, 1999.
- Slemr, F., Schuster, G., and Seiler, W.: Distribution, speciation, and budget of atmospheric mercury, *J. Atmos. Chem.*, 3, 407–434, doi:10.1007/bf00053870, 1985.
- Spuler, S., Linne, M., Sappey, A., and Snyder, S.: Development of a Cavity Ringdown Laser Absorption Spectrometer for Detection of Trace Levels of Mercury, *Appl. Optics*, 39, 2480–2486, 2000.
- Swartzendruber, P. C., Jaffe, D. A., Prestbo, E. M., Weiss-Penzias, P., Selin, N. E., Park, R., Jacob, D. J., Strode, S., and Jaegle, L.: Observations of reactive gaseous mercury in the free troposphere at the Mount Bachelor Observatory, *J. Geophys. Res.-Atmos.*, 111, D24301, doi:10.1029/2006JD007415, 2006.
- Tao, S. Q., Mazzotti, F. J., Winstead, C. B., and Miller, G. P.: Determination of elemental mercury by cavity ringdown spectrometry, *Analyst*, 125, 1021–1023, 2000.
- Tekran: Unique features of the Tekran Model 2537B, 2012, 2009.
- Venables, D., Darby, S., Pierce, A., Moore, C., Moosmüller, H., and Obrist, D.: The role of BrO in the oxidation of GEM: A chamber investigation at close-to-representative concentrations, International Conference on Mercury as a Global Pollutant, Edinburgh, Scotland, accepted presentation, 2013.
- Wang, C. J., Scherrer, S. T., Duan, Y. X., and Winstead, C. B.: Cavity ringdown measurements of mercury and its hyperfine structures at 254 nm in an atmospheric microwave plasma: spectral interference and analytical performance, *J. Anal. Atom. Spectrom.*, 20, 638–644, doi:10.1039/b504318b, 2005.
- Werle, P., Mücke, R., and Slemr, F.: The limits of signal averaging in atmospheric trace-gas monitoring by tunable diode-laser absorption spectroscopy (TDLAS), *Appl. Phys. B*, 57, 131–139, doi:10.1007/BF00425997, 1993.
- Wheeler, M. D., Newman, S. M., Orr-Ewing, A. J., and Ashfold, M. N. R.: Cavity ring-down spectroscopy, *J. Chem. Soc., Faraday Trans.*, 94, 337–351, 1998.